

1 Introduction

1.1 Motivation

Microemulsions are known as thermodynamically stable, macroscopically isotropic, and nanostructured fluid mixtures [1–6]. They consist of at least three components, made of polar, nonpolar, and amphiphilic molecules. The latter form an amphiphilic film that stabilizes the mixture. Furthermore, due to the adsorption of amphiphilic molecules into the interface, the interfacial tension between the polar and nonpolar solvents is vastly decreased [7–10]. Hence, the solubilization of the two incompatible solvents into each other becomes feasible through various choices of amphiphilic molecules, such as nonionic, anionic, and cationic surfactants, as well as different types of amphiphilic polymers.

After the first observation of microemulsions by Schulman [11,12] and Winsor [13] in the 1950s, the thermodynamic stability and complex phase behavior of microemulsion systems became the center of research in the 1970s and 1980s [1,2,14–23]. Research groups led by Kahlweit and Shinoda elucidated that the pivotal three-phase region, which consists of the microemulsion as well as water- and oil-excess phases, is generated through the interplay of the miscibility gaps in the binary side systems [14,24]. Furthermore, with various temperature- and concentration-dependent cuts through the phase prism or phase tetrahedron, they were able to show that the three-phase region marks the phase inversion, which can be traversed by tuning the temperature, salinity, or cosurfactant concentration [13,17,18]. The most famous cuts are the so-called “fish-cut” and “Shinoda-cut.” While the former presents the phase behavior of a microemulsion system as a function of temperature T and surfactant mass fraction γ at a constant water/oil ratio [2,25], the latter records the temperature-dependent phase behavior as a function of the water/oil ratio at constant γ [14].

From the late 1980s, research groups of Langevin [26–29], Scriven and Davis [30–32], Lindman, Olsson, and Wennerström [33–40], as well as Strey and Jahn [41,42] focused on the elucidation of the multifarious nanostructures formed by the amphiphilic membrane, ranging from

spherical to cylindrical and bicontinuous structures. To characterize the structure of these systems, various methods, such as small-angle neutron scattering (SANS) [4,43–45], small-angle X-ray scattering (SAXS) [46], dynamic light scattering (DLS) [26], electron microscopy [42,47], NMR self-diffusion [35,37,38,48], and electric conductivity [3], have been utilized.

Three approaches are mainly used for the theoretical description of microemulsion systems: microscopic lattice models, Landau theories, and membrane models. Since comprehensive microscopic models that consider the positions and interactions of all molecules in the microemulsion are too complex to describe the macroscopic properties of microemulsions, simplified microscopic lattice models based on lattice approximations have been used instead [49–52]. The Ginzburg-Landau model, on the other hand, describes microemulsions by the local concentration of the molecules on a somewhat larger length scale than the microscopic ones [53–57]. Thus, Teubner and Strey [53] demonstrated that the Landau theory with one order parameter could describe the scattering properties of bicontinuous microemulsions by including a negative gradient term. However, microscopic lattice models and Landau models are insufficient to describe the two-dimensional nanoscale amphiphilic film between water and oil. Over the last 30 years, membrane models based on Helfrich's bending energy [58], which considers the curvature, bending rigidity, and saddle splay modulus of surfactant membranes as well as their thermal fluctuations, have been found to describe and predict the properties of microemulsions successfully [16,40,59–63].

Due to their features, microemulsions are widely applied in industries. For instance, the ultra-low interfacial tension between water and oil is utilized in washing processes [64,65] and enhanced oil recovery (EOR) [6,66–69], multifarious nanostructures and large interfaces make microemulsions potential media for nanoporous material production [70] and catalysis [71,72], etc. In addition, because of their excellent solvent properties, microemulsions are also applicable in cosmetics and pharmaceuticals [73–75].

Recently, the so-called “surfactant-free microemulsions” [76–82] have received significant

attention. In such mixtures, the miscibility of polar and nonpolar molecules is achieved by using only weakly amphiphilic short-chain alcohols instead of conventional surfactants [77,80–82]. Kunz and Zemb discussed the thermodynamic stability of this type of mixture in terms of the balance between the hydration enthalpy and the entropy [82]. They also suggested, supported by molecular dynamics (MD) simulations, that these relatively simple mixtures are also molecularly stabilized by a weak accumulation of amphiphilic alcohols at the “highly-dynamic” nanoscopic interface between water and oil. However, the “mechanism” for achieving the thermodynamic stability of the so-called “surfactant-free microemulsions” differs significantly from that of classical microemulsions, which are stabilized by a well-defined amphiphilic film. Because the term “microemulsions” refers to these two clearly different types of thermodynamically stable mixtures, this often leads to misunderstandings in the scientific community and the literature.

Therefore, the main goal of this doctoral thesis is to systematically investigate the pathway from simple solutions to structured microemulsions and thus elaborate on the difference between thermodynamically stable surfactant-free microemulsions and classical microemulsions in **chapter 3**. **Chapter 4** then focuses on the influence of novel amphiphilic diblock copolymers on well-structured *n*-alkane microemulsions and state-of-the-art CO₂ microemulsions. Finally, **chapter 5** deals with the preparation of polyol-based CO₂ microemulsions that can be used in the production of polyurethane (PU) foams (1) and the development of a prediction tool for the formulation of balanced microemulsions using Salager’s equation (2). A detailed task description of this doctoral thesis is given in the following.

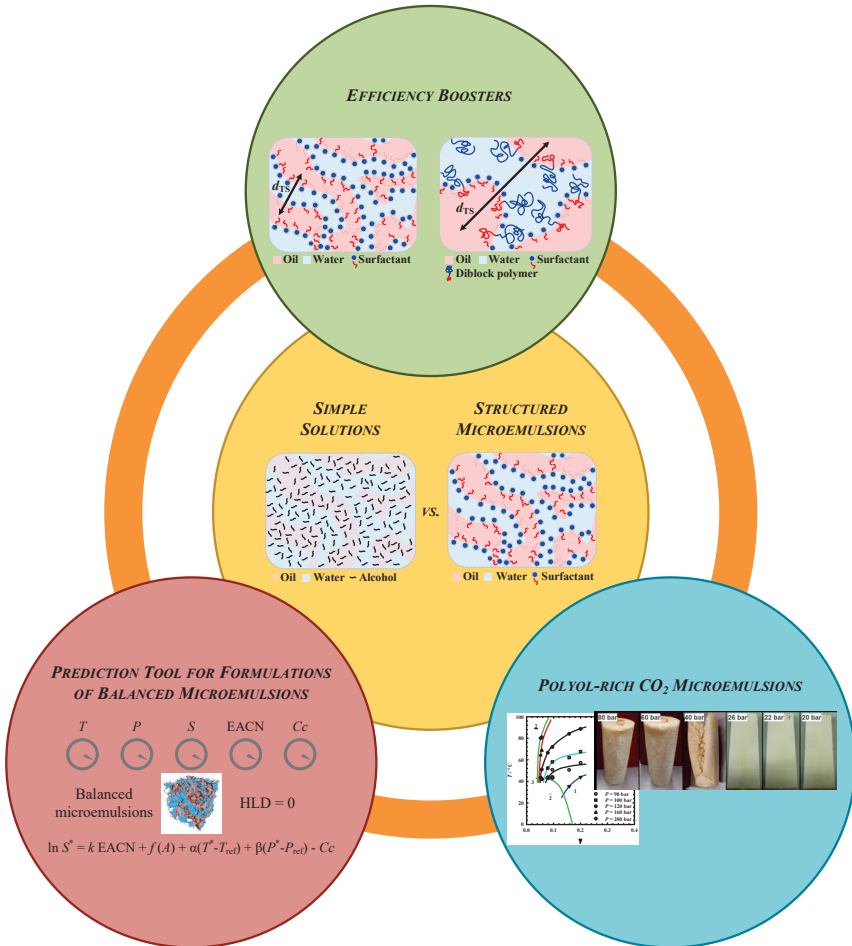


Figure 1.1: A scheme illustrating the frame of this work.

1.2 Task description

As mentioned above, this dissertation mainly aims at enlightening the difference between so-called “surfactant-free microemulsions” and classical microemulsions, which are stabilized by a well-defined amphiphilic film. The crucial role in distinguishing these two types of systems is the tricritical point (TCP), whose properties have been comprehensively studied by Kahlweit’s group in the past 40 years [2,83–86]. Those so-called “surfactant-free microemulsions” located “before” the TCP do not exhibit a three-phase triangle, while classical microemulsions located on the other side of the TCP do. In close collaboration with Prof. U. Olsson (Lund University) and Prof. R. Strey (Cologne University), **chapter 3** aims to study the phase behavior, the microstructure, and the formation of an amphiphilic film of three ternary and pseudo-ternary systems. These three systems are located not only on different sides but also at different distances from the TCP, which are (i) a rather simple solution system before the TCP with a symmetric miscibility gap and thus horizontal tie-lines, (ii) a system just after the TCP that has a three-phase triangle, and (iii) a well-structured microemulsion system on the same side as (ii) but far from the TCP. To identify the different properties of simple solutions dominated by critical composition fluctuations and structured microemulsions dominated by the amphiphilic film properties, we investigated the phase behavior, including the composition of coexisting phases by NMR and the microstructure of the three systems by light scattering, small/wide-angle X-ray scattering (SWAXS) as well as contrast variation SANS.

Having shown the difference between simple solutions and well-structured microemulsions, **chapter 4** aims at the efficiency enhancement of surfactants in stabilizing the latter. Almost 20 years ago, Jakobs et al. [87–89] found that adding small amounts of difficult-to-synthesize amphiphilic poly(ethylene propylene)-*co*-poly-(ethylene oxide) diblock polymers can boost the solubilization efficiency of medium-chain surfactants. In the search for easier-to-synthesize amphiphilic diblock polymers, two new classes of diblock polymers synthesized by Dr. L. Kunze and Dr. T. Dänzer from the group of Prof. H. Frey (JGU Mainz) were investigated for their ability

to increase the surfactant efficiency in formulating polymerizable microemulsions and CO₂ microemulsions. Therefore, the first part aims to study to what extent novel degradable polycarbonate diblock polymers poly(ethylene glycol)-*block*-poly(butylene carbonate) (mPEG-*b*-PBC) are able to increase the efficiency of nonionic surfactants to solubilize *n*-alkanes and polymerizable methacrylates within microemulsions. In the second part, we investigated whether the environmentally harmful fluorinated surfactants that have been predominantly used for the formulation of CO₂ microemulsions, which have recently received much attention [70,90,91], can be replaced by the environmentally-friendly combination of conventional hydrocarbon surfactants and novel siloxane-functionalized polycarbonate polymers poly(ethylene glycol)-*block*-poly(alkyl glycidyl ether-bis(trimethylsiloxy)methyl silane)carbonates (mPEG₄₄-*b*-P(AGE-HMTS)_{C_x}).

Finally, the goal of **chapter 5** is to utilize the acquired microemulsion expertise in two industrial applications. The first part aims to formulate foamable microemulsions for the production of nanoporous polyurethane (PU) nanofoams as a highly efficient thermal insulation material [92,93] in a collaborative project with Covestro AG, Evonik AG, FAU Erlangen-Nürnberg, JGU Mainz, Fraunhofer LBF, and CAM-D GmbH, which was funded by the BMWi. Following the principle of supercritical microemulsion expansion (POSME) procedure [70], such PU nanofoams should become feasible by expanding polyol-containing CO₂ microemulsions to which isocyanate is added shortly before the expansion for fixation. As part of this project, the task of this dissertation is to formulate new polyol-rich CO₂ microemulsions and characterize their microstructure using SANS. The second part of this chapter deals with the prediction of optimum microemulsions that is extremely useful for industrial applications, such as washing and enhanced oil recovery (EOR), based on the concept of hydrophilic-lipophilic difference (HLD) [68]. In collaboration with BASF SE, the goal is to determine the relevant parameters for optimal water/*n*-alkane microemulsions stabilized by promising extended surfactants through systematic phase behavior and electrical conductivity measurements, as well as SANS studies.

2 Fundamentals

The structure of this work is based on the development of structured microemulsions starting from the very first beginning: the mixing of water and oil with alcohol/amphiphile. Afterward, the tricritical point (TCP) is crossed, and microemulsions are formed by increasing the amphiphilicity of the amphiphile. Finally, structured microemulsions with amphiphilic films are reached. This pathway can be roughly separated into (i) systems before the TCP and (ii) systems after the TCP. Therefore, this chapter provides readers with fundamental theories regarding the critical phenomena usually observed in the system near the critical point, phase behavior of multicomponent liquid systems, including microemulsions, microstructures of microemulsions, and scattering techniques that are frequently applied to soft matter.

2.1 Phase transitions and critical phenomena

This section aims to briefly introduce the concept of phase transitions and critical phenomena in the vicinity of the critical point. The knowledge of critical phenomena helps to understand the phase behavior of the studied systems before/near the tricritical point in this work. Although many physical systems exhibit critical phenomena, fluid systems are focused on here for the sake of simplicity.

2.1.1 Phase transitions

To study the critical phenomena, one must know the relation between the critical point and the phase transition. Phase transitions are the physical processes of transitions between a state of a substance, usually marked by rapid and discontinuous changes in the properties of a system. Moreover, it has been known that the state of a pure substance can be described by an *equation of state*, an equation that correlates experimental variables, such as temperature T and pressure P . For example, in a three-dimensional space of a pure substance exhibiting coordinates as pressure P , temperature T , and density ρ , the equation of state can be written in the form as $f(P, \rho, T)$. With $f(P, \rho, T) = 0$, the surface that corresponds to the equilibrium state of the system can be

determined. When one looks at the projection of this $P\rho T$ surface onto the pressure-temperature (PT) plane shown in **Figure 2.1** (Left), phase transition boundaries between solid, liquid, and vapor states that represent the coexistence of different phases are observed. The *triple point* represents the equilibrium state in which all three phases coexist, while the end point of the liquid-vapor phase transition curve is the well-known liquid-vapor *critical point* denoted by the critical pressure P_c , the critical density ρ_c , and the critical temperature T_c . The existence of this liquid-vapor critical point implies continuous conversion between the liquid and vapor states without crossing the phase transition. Hence, there is no difference between the liquid and vapor phases.

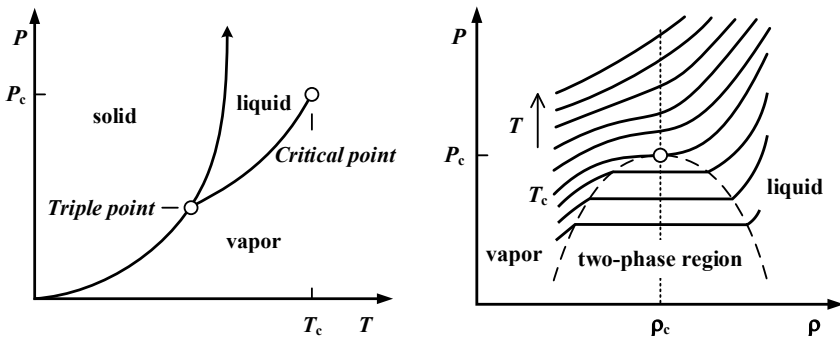


Figure 2.1: Schematic drawings of the $P\rho T$ surface projected onto (Left) the pressure-temperature (PT) plane and (Right) the pressure-density ($P\rho$) plane showing phase transition curves between three regions: solid, liquid, and vapor states of one single compound. The critical point is denoted as (P_c, ρ_c, T_c) , where P_c , ρ_c , and T_c represent the critical pressure, the critical density, and the critical temperature, respectively. Redrawn from [94].

When the $P\rho T$ surface is projected onto the pressure-density ($P\rho$) plane as in **Figure 2.1** (Right), one can see that the density difference between the liquid and vapor states varies at different temperatures. At temperatures lower than the critical temperature T_c , the density difference between the liquid and vapor phases is significant. In this region, the vapor phase can be liquified with isothermal compression. When the T_c is approached, the density difference between the vapor and liquid phases tends to be zero. Therefore, the transition from the vapor to liquid phases occurs without discontinuity of density at temperatures above T_c . This trend of

changing a quantity from non-zero to zero while increasing temperatures from $T < T_c$ to $T \geq T_c$ is a common feature related to the critical point. Moreover, different phases can be categorized by the so-called *order parameter* Ψ , which is $(\rho - \rho_c)/\rho_c$ for the liquid-vapor critical point, into *disordered phase* ($\Psi > 0$), *ordered phase* ($\Psi < 0$), and *critical temperature* ($\Psi = 0$) phases.

The physical properties of the liquid and vapor phases change dramatically during the phase transition in the vicinity of the critical point. For example, the sizes of the liquid and vapor phases start growing/fluctuating while approaching the critical point. When the sizes of these phases are comparable to the wavelength of the light, the light is scattered strongly, and thus a transparent fluid sample appears cloudy. This phenomenon is called *critical opalescence*, which Andrews discovered in 1869 [95]. The critical opalescence phenomenon is still recognized as one of the striking behavior related to the critical point.

2.1.2 Critical phenomena

In recent years, the study of critical phenomena has paid more attention to the critical exponents, which describe physical quantities of interest near the critical point. As mentioned in the previous section, the order parameter tends to zero when close to the critical point. To describe the behavior near the critical point of a general function $f(\varepsilon)$, a dimensionless variable is first defined as

$$\varepsilon \equiv \frac{T - T_c}{T_c} \quad (2-1)$$

with T_c represents the temperature at the critical point. This variable $\varepsilon \rightarrow 0$ when $T \rightarrow T_c$. Associated with the function $f(\varepsilon)$, the critical exponent λ can be defined as

$$\lambda \equiv \lim_{\varepsilon \rightarrow 0} \frac{\ln|f(\varepsilon)|}{\ln|\varepsilon|} \quad (2-2)$$

The relation between the critical exponent λ and the function $f(\varepsilon)$ is frequently denoted by

$$f(\varepsilon) \sim \varepsilon^\lambda \quad (2-3)$$

where the function $f(\varepsilon)$ is expressed as

$$f(\varepsilon) = A\varepsilon^\lambda(1 + B\varepsilon^x + \dots) [x > 0] \tag{2-4}$$

In the case of $T < T_c$, the critical exponent is denoted as λ' and defined as

$$\lambda' \equiv \lim_{\varepsilon \rightarrow 0} \frac{\ln|f(-\varepsilon)|}{\ln|\varepsilon|} \tag{2-5}$$

where the function $f(\varepsilon)$ is expressed as

$$f(\varepsilon) \sim (-\varepsilon)^{\lambda'} \tag{2-6}$$

The existence of critical exponents is essential mainly because of two reasons. First, critical exponents can be easily obtained from the slopes of log-log plots of experimental data when close to the critical point. Hence, critical exponents are easier to be determined, while the complete function $f(\varepsilon)$ might not be. Second, many relations between critical exponents arise from fundamental thermodynamic and statistical mechanical considerations and thus go beyond any systems. The most common critical exponents for fluid systems, such as α , β , γ , and ν , that are used for different thermodynamic properties are listed in **Table 2.1**.

Table 2.1: List of common critical exponents for fluid systems [94].

Exponent	Definition for fluid systems	Quantity
$\alpha^{(\prime)}$	$C_V \sim (-\varepsilon)^{-\alpha'}$ ($\varepsilon < 0$) $C_V \sim \varepsilon^{-\alpha}$ ($\varepsilon > 0$)	specific heat capacity at V_c and P_c
β	$(\rho_l - \rho_v) \sim (-\varepsilon)^\beta$	liquid-vapor density difference at P_c
$\gamma^{(\prime)}$	$K_T \sim (-\varepsilon)^{-\gamma'}$ ($\varepsilon < 0$) $K_T \sim \varepsilon^{-\gamma}$ ($\varepsilon > 0$)	isothermal compressibility at P_c
δ	$(P - P_c) \sim \text{sgn}(\rho_l - \rho_v) \rho_l - \rho_v ^\delta$	critical isotherm
$\nu^{(\prime)}$	$\xi \sim (-\varepsilon)^{-\nu'}$ ($\varepsilon < 0$) $\xi \sim \varepsilon^{-\nu}$ ($\varepsilon > 0$)	correlation length at P_c
η	$G(r) \sim r ^{-(d-2+\eta)}$	pair correlation function at $\varepsilon = 0$ ($d = \text{dimensionality}$)

For example, the classic Guggenheim plot in **Figure 2.2** shows the coexistence curve of liquid and vapor for eight different simple fluids as a function of reduced temperature and density. All data points fall onto one curve agree with the *Law of corresponding states*, which states that all